ACS chemical biology

Letters

Cite This: ACS Chem. Biol. XXXX, XXX, XXX−XXX

Rescuing the Rescuer: On the Protein Complex between the Human Mitochondrial Acyl Carrier Protein and ISD11

María Georgina Herrera,[†] María Florencia Pignataro,[†] Martín Ezequiel Noguera,[†] Karen Magalí Cruz,[†] and Javier Santos*[,†]

[†]Institute of Biological Chemistry and Physical Chemistry, Dr. Alejandro Paladini (UBA-CONICET), University of Buenos Aires, Junín 956, C1113AAD Buenos Aires, Argentina

Supporting Information

ABSTRACT: Iron−sulfur clusters are essential cofactors in many biochemical processes. ISD11, one of the subunits of the protein complex that carries out the cluster assembly in mitochondria, is necessary for cysteine desulfurase NFS1 stability and function. Several authors have recently provided evidence showing that ISD11 interacts with the acyl carrier protein (ACP). We carried out the coexpression of human mitochondrial ACP and ISD11 in *E. coli*. This work shows that ACP and ISD11 form a soluble, structured, and stable complex able to bind to the human NFS1 subunit modulating its activity. Results suggest that ACP plays a key-role in ISD11 folding and stability *in vitro*. These findings offer the opportunity to study the mechanism of interaction between ISD11 and NFS1.

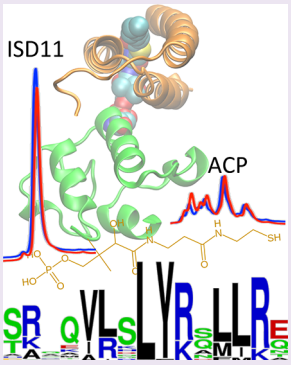

Iron sulfur (Fe−S) clusters play an essential role in multiple biochemical processes.[1,2] Mutations of proteins involved in the biosynthesis of the Fe−S cluster in mitochondria result in severe metabolic diseases.[3−10] These cofactors are synthesized by a complex machinery involving several proteins: the desulfurase NFS1; the ISD11 protein, also known as LYRM4 (Figure S1), a member of the LYR family exclusive of eukaryotic organisms;[11] frataxin (FXN), which is a positive regulator of desulfurase activity in mammals[12−15]and also binds iron; ferredoxins (FDX1 and FDX2[16]), which provide electrons for cluster synthesis; and the scaffold protein ISCU,[17] the platform where the clusters are assembled. In particular, the loss of FXN and ISCU functionality leads to Friedreich ataxia and ISCU myopathy, respectively, which are the most prevalent pathophysiological disorders associated with a deficiency in Fe−S cluster biosynthesis in human mitochondria.[4,8]

In addition, dissociation and cluster transfer from ISCU to intermediate protein carriers (glutaredoxin 5, GLRX5, among others)[18,19] are intricate processes that require dedicated chaperone systems like HSP70-HSP40.[20] Several structural biology aspects of this biosynthetic complex were recently elucidated,[21,22] providing a significant advance in the study of the architecture and function of the eukaryotic systems. Particularly, the three-dimensional structure of ISD11 was determined, which is a small 10.8 kDa protein (human variant, isoform 1) essential for NFS1 activity and stability, even though it does not directly participate in catalysis.[21,23,24] In fact, in the absence of ISD11, NFS1 is prone to aggregate, whereas the clinically relevant mutation R68L of ISD11 reduces affinity by NFS1, inhibiting the consolidation of a stable complex and compromising Fe−S cluster biogenesis, leading to mitochondrial dysfunction.[25,26]

One of the main problems that has delayed the conformational study of ISD11 is the high tendency of this protein to aggregate when it is expressed in *E. coli*, leading to the impossibility of obtaining a properly folded protein at high concentrations, necessary for structure determination by NMR[9] or X-rays. The understanding of this behavior is not obvious from the analysis of the amino acid sequence or residue composition. In this regard, this protein is very rich in positive-charged residues, with a theoretical isoelectric point of 10.7. The *ab initio* model of the tertiary structure suggests a compact structure formed by three α-helices that superimpose very well with the obtained structure.

More importantly, the X-ray structure of the NFS1-ISD11 complex[22] reveals how its folded conformation may be stabilized. This crystal structure, curiously, includes a protein passenger. Desulfurase NFS1 and ISD11 present additional interaction with another protein, the acyl carrier protein (ACP) from *E. coli*, which is copurified with ISD11.[22,24] Contrarily to ISD11, ACP is very rich in acidic side chains; therefore, its theoretical isoelectric point deduced from amino acid composition is very low: pI = 4.1. Unexpectedly, the acyl chain, which modifies the phosphopantetheine moiety (4-PP) covalently bound to an invariant Ser residue of ACP, is directly interacting with the core of ISD11. In fact, ISD11 shows a hydrophobic groove that is penetrated by the acyl chain, which,

Received: February 23, 2018
Accepted: May 8, 2018
Published: May 8, 2018

DOI: 10.1021/acschembio.8b00184
ACS Chem. Biol. XXXX, XXX, XXX−XXX

in turn, complements the core of the protein. Moreover, the passenger ACP shows a large interaction surface with ISD11 that may also help it to remain in a soluble form. Given the high sequence identity between eukaryotic and bacterial ACP proteins, it is not surprising that ACP from *E. coli* interacts with proteins from the mammalian Fe−S biosynthetic complex. Furthermore, in the yeast *Yarrowia lipolytica*, ACP (ACPM1) was found in the mitochondrial matrix both as a free protein and in complex with the soluble ISD11-NFS1 complex.[27]

First, we tried to produce ISD11 alone in *E. coli* BL21 cells. Even though the protein was overexpressed at high yields, it was mainly found in the inclusion body fraction. All attempts of our group to produce soluble ISD11, in the absence of partners, have failed to date. In addition, refolding of the protein following purification under denaturing conditions, by dialysis or dilution, proved to be highly inefficient. Therefore, we tried to refold the protein in the presence of low-to-moderate detergent concentrations, which may be thought of as mimetics of the acyl chain covalently bound to ACP and intimately inserted in ISD11 as seen in the crystal structure of the NFS1-ISD1 complex.[22] We evaluated N-dodecyl β-D-maltoside (DDM) and sodium dodecyl sulfate (SDS) detergents and observed that refolding by dilution from 8.0 to 0.4 M urea allows us to obtain 10 μM concentration of soluble and apparently structured ISD11, as judged by far-UV CD spectra. However, we were not able to reach higher concentrations.

In a context in which ISD11 has been proposed as the rescuer of the eukaryotic desulfurase NFS1, is ACP the rescuer of ISD11? In that line of thinking, it was shown that mitochondrial ACP, which is a central subunit in mitochondrial fatty acid synthesis, is at the same time a subunit associated with the eukaryotic Fe−S biosynthetic complex, and this function is dependent on the post-translational modification of the invariant Ser residue with the 4-PP-acyl chain.[28] Thus, we wondered if the interaction between human ACP and ISD11 is able to stabilize the folded state of the latter maintaining the protein complex soluble. We reasoned it may depend on the capability of the host to post-translationally modify recombinant ACP with the 4-PP-acyl chain. Consequently, and given the evidence favoring ACP-ISD11 interaction, we decided to evaluate the effect of coexpression in *E. coli* BL21 of human mitochondrial ACP (10.0 kDa) with ISD11 (12.4 kDa) on ISD11 solubility, conformation and stability.

After protein induction and cell disruption, the analysis of soluble and insoluble cellular fractions by SDS-PAGE confirmed that more than 50% of ISD11 remained soluble (Figure 1A). Soluble ACP-ISD11 was easily purified by means of NTA-Ni^{2+}, taking advantage of an N-terminal His-tag (His6) in the ISD11 protein. Remarkably, the complex reached a concentration of 70 μM following purification, and after dialysis to remove imidazole, it was concentrated up to 200 μM by diafiltration. The fact that ACP and ISD11 were copurified under high ionic-strength conditions suggests that a specific and high-affinity complex was formed. This is in concordance with the crystal structure of the *bacterial* ACP in complex with human ISD11 and NFS1, in which the covalently bound acyl 4-PP moiety of ACP is inserted into the core of ISD11, tightly interacting with it. Interestingly, success in the consolidation of the ACP-ISD11 complex depended on the capability of two *E. coli* enzymes (4′-PP transferase and ACP S-acetyltransferase) to recognize and modify the human mitochondrial variant of ACP. It is worthy of note that the tertiary structures of both proteins are very similar (PDB IDs: 2DNW and 4USR or 5WGB, for human and *E. coli*, respectively), with a RMSD = 1.5 Å (264 backbone atoms involved).

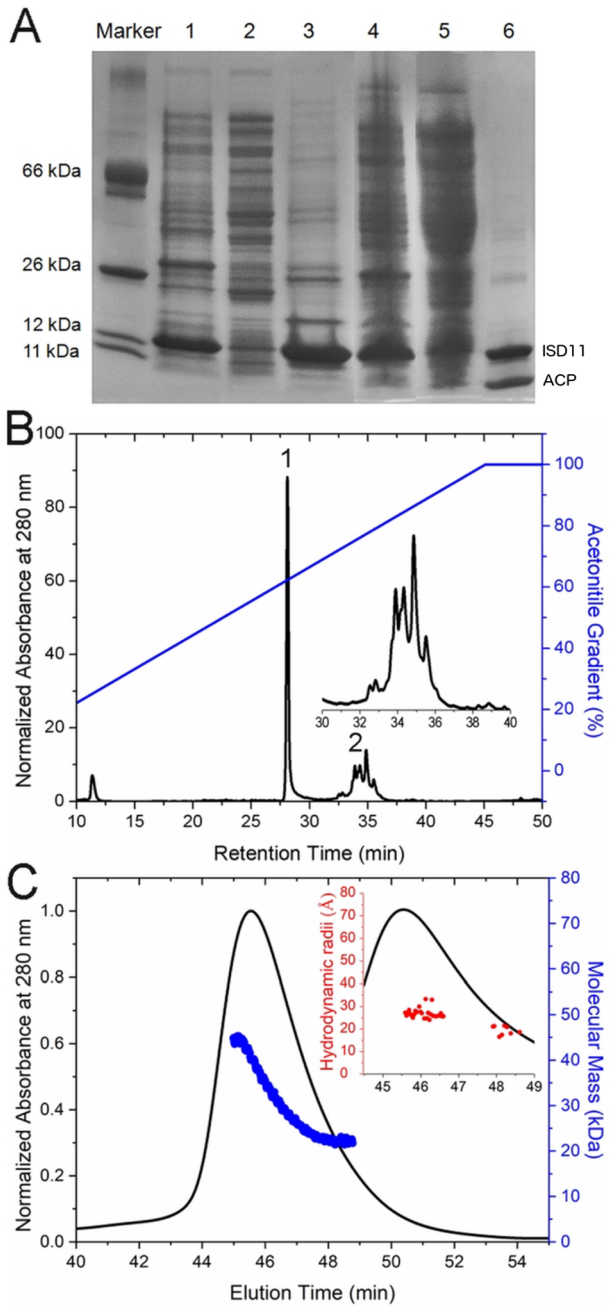

Figure 1. Analysis of the ACP-ISD11 complex. (A) SDS-PAGE analysis showing insoluble and soluble fractions from cultures overexpressing ISD11 alone (lanes 1 and 2) and purified ISD11 (under denaturant conditions, line 3), or insoluble and soluble fractions from cultures overexpressing ISD11 and ACP (coexpression, lanes 4, 5) and purified ACP-ISD11 complex (under native conditions, line 6). (B) Elution profile of a reversed phase HPLC of ACP-ISD11 complex (black). A C4 HPLC column was used, and elution was carried out throughout the gradient from 0 to 100% of acetonitrile (blue). Inset shows a zoomed region of the chromatogram corresponding to the elution of ACP. (C) Hydrodynamic behavior of the ACP-ISD11 protein complex. SEC profiles are shown (black); the calculated molecular mass values using UV and MALS detectors are in blue. The inset shows in red the R_h values obtained by DLS.

The ACP-ISD11 complex was analyzed by C4-reversed phase HPLC (Figure 1B). While ISD11 eluted as a single well-defined

DOI: 10.1021/acschembio.8b00184
ACS Chem. Biol. XXXX, XXX, XXX−XXX

peak (assigned as 1 at ~64% ACN), ACP eluted in multiple peaks at higher ACN concentrations (assigned as 2 in the range 75−82%), revealing that the ACP was highly heterogeneous, most likely due to post-translational modifications that this protein undergoes during *E. coli* BL21 expression. By integrating peak areas corresponding to ACP and ISD11 and taking into account the absorption coefficients, a 1:1 stoichiometry was inferred (ACP: ISD11 molar ratio was 0.97 ± 0.34). N-terminal sequencing (automated Edman degradation) of the protein corresponding to each peak established unambiguously the identity of both human ACP and ISD11 (sequences for ACP and ISD11 were SDMPPLTLE and MHHHH, respectively, Figure S2). Remarkably, proteins had a very high degree of purity (>98%), and no other proteins were detected. The isolated proteins were also analyzed by ESI-MS (Figure S3), and the mass charge relation values corresponding to the most important ions are shown in Table S1. The observed masses are in agreement with the ones expected for different acylated forms of holo-ACP: 10 720 ± 3 Da can be assigned to the tetradecanoate, whereas 10 735 ± 3 Da may be assigned to 3-hydroxy-tetradecanoate and 3-keto-tetradecanoate, previously detected for mitochondrial ACP-ISD11 protein complexes,[27] and 10 762 Da can be assigned to the 16-carbon acyl-chain, previously observed for the ISD11 complex with *E. coli* ACP.[22] On the other hand, 10 789 Da might correspond to longer acyl chains.

The hydrodynamics properties of the purified complex ACP-ISD11 were explored through size-exclusion chromatography and light-scattering analysis (Figure 1C). The proteins mainly eluted as a single peak. However, multiangle light scattering analysis indicated the presence of species of 44.0 ± 0.6 and 22.1 ± 0.4 kDa, compatible with the presence of heterotetramer and heterodimers in rapid equilibrium. This result showed that ACP maintained soluble ISD11 even at high protein concentrations. In addition, the hydrodynamic radii observed were in the range of R_h = 27 ± 2 to 20 ± 3 Å, compatible with a folded conformation of tetramers and dimers (theoretical values are 27 and 22 Å, respectively, Figure 1C). By contrast, the expected values calculated from correlations between the number of residues and R_h[29] for unfolded or intrinsically disordered proteins of these molecular masses are 61 and 52 Å for the tetramer or 42 and 36 Å for the dimer, respectively.

We studied the conformation of the ACP-ISD11 complex by circular dichroism spectroscopy (CD). Also, ISD11 refolded in the presence of DDM, or SDS was analyzed. High CD signals in the far-UV region at 208 and 222 nm were observed for the three samples, an indication of substantial α-helical content (Figure 2A). The analysis of CD spectra using BeStSel[30] showed 50% of a α-helical structure, in agreement with the 60% determined from the crystal structures of ISD11 and ACP using Stride.[31] Furthermore, as a signature of the tertiary structure, well-defined CD bands were observed between 255 and 310 nm in the near-UV CD spectra (Figure 2B). These bands reported the presence of asymmetry in the environments of the aromatic residues. The same analysis was achievable for ISD11 refolded in the presence of DDM (Figure 2B). However, with this detergent, significantly lower CD signal intensities were acquired compared with those of the ACP-ISD11 complex. In the presence of SDS, it was not possible to characterize ISD11 refolded due to the low protein concentration reached.

Cooperativity is an important feature of well folded proteins with consolidated secondary and tertiary structures. This feature was evaluated by temperature-induced unfolding

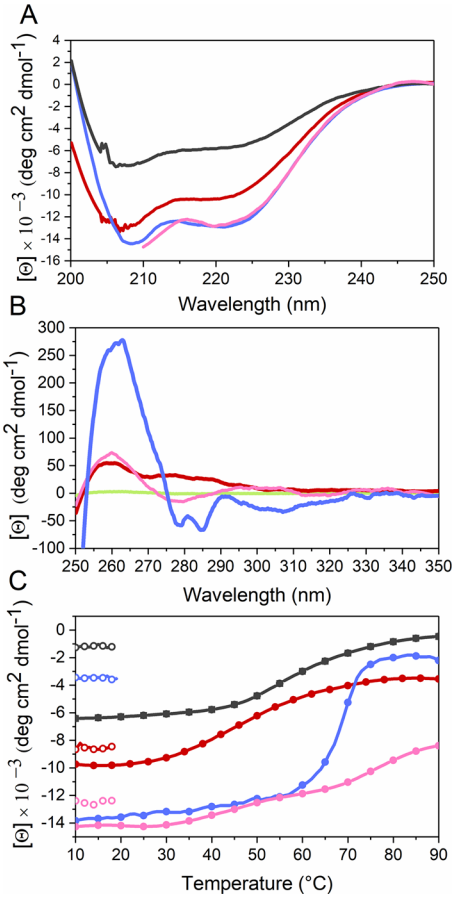

Figure 2. Spectroscopic analysis and stability of ISD11 and ACP-ISD11. Far-UV CD (A) and near-UV CD spectra (B) of isolated, refolded ISD11 in 20 mM Tris-HCl, 200 mM NaCl at pH 9.0 plus 1 mM DDM or 0.45 mM SDS (black and red, respectively), or ACP-ISD11 complex in 100 mM phosphate, 300 mM NaCl at pH 8, in the absence (blue) or presence (pink) of 1.0 M GdmHCl. The spectrum corresponding to the buffer is in green. (C) Temperature-induced unfolding of proteins. Colors are the same as in A. Denaturation was followed by the change in the far-UV CD signal at 220 nm under 100 mM phosphate and 300 mM NaCl at pH 8.0. The signals acquired after uncontrolled cooling of the samples are shown as empty symbols.

experiments followed by the change in CD signal at 220 nm (Figure 2C). From a qualitative viewpoint, the complex ACP-ISD11 proved to be significantly stable to temperature-induced unfolding and/or temperature-induced aggregation (apparent T_m= 68.4 ± 1 °C). In addition, the transition occurred in a narrow range of temperatures, showing that they form a single folding unit.

Denaturation of ACP-ISD11 was also studied using Sypro Orange dye, a probe that binds to unfolded proteins.[32] In agreement with CD experiments, our results suggested one main conformational transition for the ACP-ISD11 complex (Figure S4) and cooperative unfolding with a high apparent T_m (64.3 ± 0.6 °C). Unfortunately, this experiment could not be done with refolded ISD11 because the detergent binds the fluorescent probe. These results are in agreement with crystallographic evidence, which shows that human ISD11 has a large interacting surface with ACP from *E. coli*, in which electrostatic forces play a key role.[21] Similar interactions may be established with the human variant of ACP (human and *E. coli* ACP has approximately 70% of sequence identity and 90% of similarity in the interacting α-helix of ACP, Figure S5, residues

DOI: 10.1021/acschembio.8b00184
ACS Chem. Biol. XXXX, XXX, XXX−XXX

111−126). In this regard, Figure 3 shows a model for the human ACP in complex with ISD11. Electrostatic complementarity is a notable feature of the interaction between these proteins and appears as a recurring theme in experimentally determined structures of the ACP complexes with other LYR-family proteins (Figure 3C). On the other hand, we were unable to perform a quantitative analysis of the unfolding profiles given the irreversibility of the process as judged by the values of the CD signal at 220 nm after cooling the protein samples. Low concentrations of a chaotropic agent to the ACP-ISD11 protein sample may be enough to weaken intermolecular interactions between subunits. In agreement with this hypothesis, when 1.0 M GdmCl was added to the protein sample, two unfolding transitions were observed (Figure 2). Furthermore, 1.0 M GdmCl resulted in a higher signal recovery after cooling the sample.

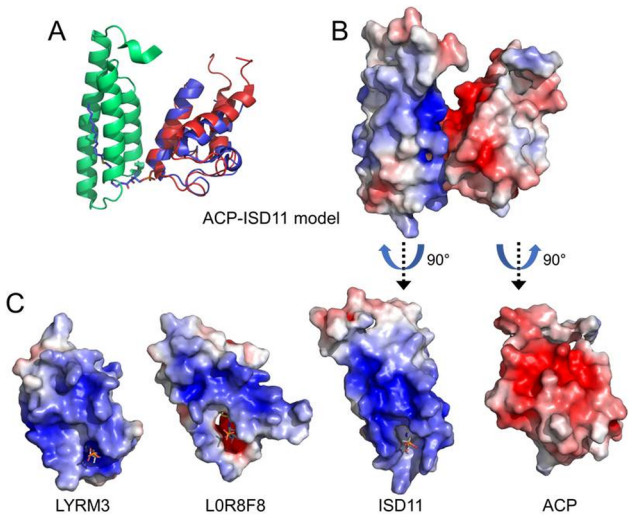

Figure 3. Modeled structure of the ACP-ISD11 complex and conservation of surface electrostatics. (A) The crystal structure of the ISD11 and bacterial ACP complex is depicted as a ribbon model in green (ISD11) and blue (ACP), with the 4-PP moiety shown in sticks. The NMR structure of human ACP (red) is shown superimposed to the bacterial variant, following structural alignment of the highly conserved α helix that interacts with ISD11. (B) Surface electrostatic representation of the modeled human ACP-ISD11 complex is shown in the same orientation as in panel A. Electrostatics were calculated using APBS and color scale ranges from +5 (blue) to −5 kT/e (red). (C) Both subunits of the complex in panel B were rotated outward (arrows), and surface electrostatics is shown using the same scale as in panel B. Additionally, representations of the LYR subunits taken from structures of mitochondrial respiratory (PDB 5XTH) or ribosome (PDB 5OOM) complexes, LYRM3 and L0R8F8, respectively, are shown in the same orientation as the ISD11 subunit, highlighting conservation of surface electrostatics. The 4-PP moiety is shown as sticks.

Interestingly, ISD11 refolded in the presence of 1.0 mM DDM or 0.45 mM SDS exhibited unfolding transition profiles compatible with the decrease in the secondary structure content (Figure 2C). However, cooperativity (inferred from the change in the CD signal at 220 nm with the temperature variation) was significantly reduced as well as the apparent T_m (~40.8 and ~53.4 °C for DDM and SDS, respectively), additionally suggesting low resistance to thermal denaturation. Interestingly, Yan and co-workers were able to express ISD11 in a soluble form as a fusion protein with an N-terminal GST-tag.[33] They observed that ISD11 exists in different oligomeric states in solution, as a mixture of monomer, dimer, and tetramer; also they suggested that the high T_m value that characterizes the ISD11 denaturation profile might be the consequence of extra stabilization that results from the oligomeric state of the protein.[33]

To further explore the conformation of ACP-ISD11, we performed a proteolysis assay using chymotrypsin (methodological details may be found in Supporting Information, Figures S6−S8). Nearly 40% of ISD11 was resistant after 1 h of incubation with the protease, suggesting that the protein is properly folded. But the overnight incubation resulted in complete degradation of ISD11; however, more than 80% of ACP remained intact. This behavior is in agreement with differences in accessibility of the aromatic residues of these proteins in the native state (Figures S6 and S7). At this stage of the work, we cannot exclude that, additionally, ISD11 might exhibit high flexibility, even in the context of the ACP-ISD11 heterodimer.

Remarkably, when ISD11 was refolded in the presence of 1 mM DDM (in the absence of ACP), higher sensitivity to proteolysis was detected, compared to that observed for ISD11 in the context of the ACP-ISD11 complex (Figures S9 and S10). This result is in agreement with the low cooperativity observed in unfolding profiles and suggests an unstable tertiary structure, which may be indicative of the stabilization conferred to ISD11 by intermolecular interactions mediated by the holo ACP protein.

We tested the functionality of the ACP-ISD11 complex. First, we explored the capability of this complex to interact with the NFS1 desulfurase. To this end, a solid phase binding assay linked to the detection of the latter was carried out using a monoclonal antibody (mAB) that recognizes the RGSHHHH epitope present in the N-terminal region of the recombinant variant of NFS1. Results showed that when the ACP-ISD11 complex was immobilized in the plate, the complex was able to interact with NFS1 (Figure 4A). On the other hand, neither the ISD11 nor the ACP-ISD11 were recognized by this mAB when incubated in the absence of NFS1. Also, a control of blocking in the absence of ACP-ISD11 was performed to rule out unspecific binding of NFS1. Interestingly, when ISD11 folded in the presence of DDM was fixed to the plate, ISD11 was able to interact with NFS1, but to a lesser extent. Results indicate that ACP-ISD11 preserved all the conformational features important for NFS1 binding, and possibly some of them were absent in the refolded ISD11 (in the presence of DDM). When a fixed ACP-ISD11 quantity was immobilized and titrated with different NFS1 concentrations, a hyperbolic curve was observed (Figure 4A, inset), indicating that the binding of NFS1 to the ACP-ISD11 complex was due to a specific interaction. Taking advantage of the fact that ACP and ISD11 proteins do not contain tryptophan in their amino acid sequences, and given that the addition of ACP-ISD11 to NFS1 produced a decrease in tryptophan emission of the latter, we carried out an equilibrium-titration experiment of NFS1 with ACP-ISD11 (Figure 4B). Results were compatible with a dissociation constant (K_D) in the micromolar range (2−5 μM); however, as the ACP-ISD11 heterodimer is in equilibrium with an heterotetrameric form, and the proportion of species depends on the protein concentration that varies during titration, the interpretation of this result is not unequivocal.

As the ACP-ISD11 complex was able to bind NFS1, we explored the capability of the complex to modulate NFS1

DOI: 10.1021/acschembio.8b00184
ACS Chem. Biol. XXXX, XXX, XXX−XXX

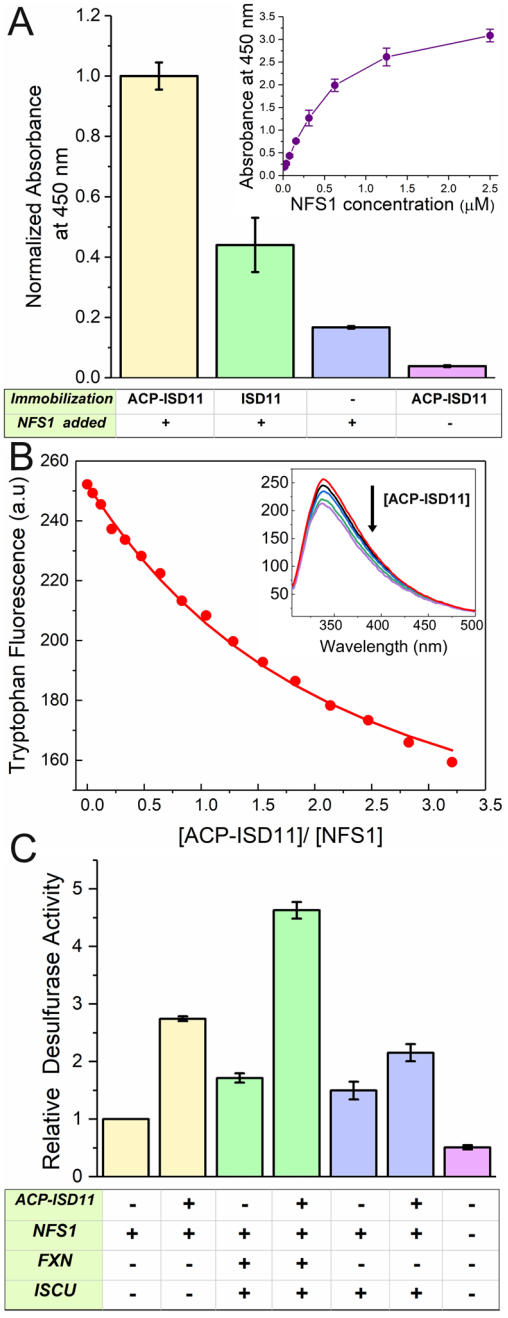

Figure 4. Functionality of the ACP-ISD11 protein complex. (A) Interaction assay between the ACP-ISD11 complex and NFS1. ACP-ISD11 (6 μM) or refolded ISD11 in DDM (6 μM) were bound to a NUNC plate. After a blocking step, plates were incubated for 1 h with or without NFS1 (5.5 μM). After that, the plate was washed and then incubated with an anti RGSHHHH peroxidase-conjugated antibody. Plates were revealed using the TMB peroxidase substrate. Inset: The NFS1 titration assay of the ACP-ISD11 complex immobilized in a plate as described above with 4 μM solution of ACP-ISD11. (B) Titration of NFS1 with ACP-ISD11 followed by Trp fluorescence at 336 nm. NFS1 concentration was 1.6 μM and ACP-ISD11 was added up to 3.2 equiv. The experiment was performed at 25 °C. Excitation wavelength was 295 nm and emission spectra were acquired between 305 and 500 nm. The continuous line represents the best fitting, considering one binding site per NFS1 molecule. Inset: emission spectra corresponding to 1.6 μM NFS1 in the presence of 0, 0.5, 1.2, 2.5, and 3.5 μM ACP-ISD11. The arrow indicates the increase in the ACP-ISD11 concentration. (C) Cysteine desulfurase activity of NFS1 depends on ACP-ISD11. Sulfide production was measured by the methylene blue method. Protein concentrations were 1.0 μM NFS1, 3.0 μM FXN, 3.0 μM ISCU, and 1.0 μM ACP-ISD11. Samples were supplemented with 10 μM PLP, 2 mM DTT, and 1.0 μM Fe^{2+} (final concentrations). The reaction was started with the addition of 1.0 mM cysteine, and samples were incubated at RT for 30 min. Results are expressed as the fold of activity of the NFS1 sample alone. Error bars correspond to the standard deviation of three experiments.

enzymatic activity. It was shown that FXN binds to a NFS1-ISD11-ISCU protein complex to yield the core machinery for Fe−S cluster biosynthesis and to produce the allosteric activation of NFS1.[12] FXN interaction severely changes the K_M for cysteine and the catalytic efficiency of the cysteine desulfurase; additionally, FXN accelerates the rate-limiting step of sulfur transfer in the synthesis of [2Fe-2S] clusters.[34,35] Thus, a desulfurase reaction was evaluated in the presence or in the absence of ACP-ISD11 and several other conditions (e.g., in the presence or absence of FXN). Results showed that cysteine desulfurase activity of NFS1 increased in the presence of the ACP-ISD11 complex. The addition of ISCU to ACP-ISD11-NFS1 decreases desulfurase activity, in agreement with previous results that suggested a slight decrease of the k_{cat} of NFS1 upon interaction with ISCU,[36] whereas the activation mediated by FXN depended on the presence of the ACP-ISD11 complex (Figure 4C). As stability and function of NFS1 depends on ISD11, and considering that (i) solubility of the latter depends on its interaction with ACP and (ii) the interaction between ACP and ISD11 depends on post-translational modification of ACP, it seems that post-translational modification of ACP is one of the key factors necessary for iron−sulfur cluster biosynthesis. This binding mode can also be observed for interaction between mitochondrial ACP and other members of the LYR protein family: LYRM3 (Figure 3C) and LYRM6, which interact with respiratory complex I in *Y. lipolytica*, *A. thaliana*, *T. brucei*, and *H. sapiens*[37,38] and protein L0R8F8 (Figure 3C), an assembly factor of mammalian mitochondrial ribosomes.[39] In particular, deletion studies in *Y. lipolytica* revealed that mitochondrial ACP2 is essential for complex I assembly/stability,[40] whereas mitochondrial ACP1 may be involved in controlling the catalytic activity of complex I, and the loss of this protein paralyzes ubiquinone reductase activity,[41] Interestingly, Boniecki and co-workers observed that, under certain metabolic conditions during *E. coli* expression, the enzymatically active form of the NFS1-ISD11 complex can be obtained without ACP subunits;[21] however, it is not clear whether the ternary complex (ACP-ISD11-NFS1) is more stable than the binary form (NFS1-ISD11) and if these alternative forms are equally important for biological function.

In this work, we found that the solubility of ISD11 is dramatically increased by coexpression with the human mitochondrial ACP. This fact suggests that ISD11 conformation is stabilized when interactions involving ACP and its covalently bound acyl moiety are established. Our results indicate that in the absence of ACP, but in the presence of detergents, such as SDS or DDM, the secondary structure of ISD11 may be induced in solution. However, even in the presence of detergents, ISD11 showed a high tendency to aggregate, preventing the attainment of high protein concentrations. The opportunity of having a soluble and structured ACP-ISD11 complex opens up the possibility for studying the dynamics of ISD11 in the absence of NFS1 and the interaction

DOI: 10.1021/acschembio.8b00184
ACS Chem. Biol. XXXX, XXX, XXX−XXX

mechanism of these proteins. Moreover, understanding ACP-ISD11 structure consolidation allows for re-engineering ISD11 to design new variants with the capability of altering cell function, interfering with the metabolic pathway in eukaryotes and expanding the LYRM network in these organisms but also in bacteria, in which the LYR family is completely absent.[11]

METHODS

Protein Expression and Purification. DNA was optimized for protein expression in *E. coli* BL21 (DE3) by BIO BASIC Inc. In all cases, protein expression was induced with 1% lactose (final concentration), and cells were disrupted by sonication. Expression of the human mitochondrial ISD11 carrying an N-terminal His6 tag was induced at 37 °C (4 h at 250 rpm). Protein was purified from the insoluble fraction under unfolding conditions (urea 8.0 M) using the CAPTOQ column first and a Ni^{2+}-NTA-agarose column second. Most of the ISD11 was eluted with 200 mM imidazole. Once purified and dialyzed, ISD11 was refolded by dilution (1:20) in the presence of detergents (SDS or DDM). After refolding, a subsequent dialysis step was carried out to remove the remaining urea. Expression of the human mitochondrial ACP-ISD11 complex was carried out in a similar fashion as ISD11 alone, but the complex was purified from the soluble fractions under native conditions by Ni^{2+}-NTA-agarose chromatography. Most of the recombinant protein was eluted with 500 mM imidazole. Expression of human NFS1 (NFS1Δ55) was carried out overnight at 20 °C (at 250 rpm), in the absence of the ISD11 subunit, and purification was performed from the soluble fraction using a Ni^{2+}-NTA-agarose column. The N-terminus of NFS1 included a RSGHHHHHH tag for purification and antibody recognition. The recombinant protein was eluted with 500 mM imidazole. In all cases, once purified, proteins were extensively dialyzed against the desired buffer. Protein sequences are shown in the Supporting Information.

Light-Scattering Measurements and Reversed Phase HPLC. The oligomerization state and molecular mass determinations were performed by multiple-angle laser light-scattering (MALLS) using miniDawn (Wyatt Technology) coupled to a size-exclusion Superose-12 column (GE Healthcare), at RT and at a 0.3 mL/min flow rate. Hydrodynamic radii were calculated from the translational diffusion coefficient measured using a DLS module (Wyatt Technology). Data analysis was performed using Astra 6.0 software (Wyatt Technology). Protein concentration was 200 μM, and the buffer was 20 mM Tris-HCl and 300 mM NaCl, at pH 7.5.

The purity and heterogeneity of protein samples were analyzed using a HPLC system (Rainin Dynamax NY) equipped with a column proto 300 C4 5 μm 250 × 4.6 mm (Higgins Analytical, Inc.) that was equilibrated in 0.05% aqueous TFA. Elution was carried out throughout a gradient from 0 to 100% of acetonitrile (ACN). All HPLC solvents included 0.05% TFA. Flow was 0.7 mL/min, and detection was carried out at 280 nm. Average pressure during the run was 0.7 kPSI.

Spectroscopic Characterization of Proteins and Unfolding Experiments. Protein concentration was estimated using the extinction coefficients deduced from amino acid sequences for ACP and ISD11; ε_{280nm} was 5960 and 8940 M^{-1} cm^{-1}, respectively (1 mg mL^{-1} of protein yields 0.579 (for ACP) and 0.719 (for ISD11) absorbance at 280 nm). Circular dichroism (CD) measurements were carried out with a Jasco J-810 spectropolarimeter. Near-UV and far-UV CD spectra were collected using cells of 1.0 and 0.1 cm path length, respectively. Data were acquired at a scan speed of 20 nm min^{-1}, and at least five scans were averaged. Protein concentration was 10 μM in the case of the DDM sample (20 mM Tris-HCl, 200 mM NaCl, 1 mM DDM and pH 9.0) and 8.3 μM in the case of the SDS sample (20 mM Tris-HCl, 200 mM NaCl, 0.45 mM DDM and pH 9.0) for far- and near-UV CD measurements. For the ACP-ISD11 complex, protein concentration for far UV-CD was 14 μM, and the near-UV was 56 μM.

Temperature-induced unfolding was monitored by the circular dichroism signal at 222 nm using a bandwidth of 2 nm. The buffer was 100 mM sodium phosphate and 300 mM NaCl at pH 8.0. Protein concentration was 3.2 μM in the case of the ACP-ISD11 complex. For the isolated ISD11 refolded in DDM or SDS, protein conditions were the same as described above. The temperature was varied from 4° to 90 °C, at a constant rate of 1 °C min^{-1}, sampling at 1 °C intervals, and a 1.0 cm cell path length was used.

ACP-ISD11 NFS1 Binding Assay and Enzyme-linked Immunodetection of the Ternary Complex. The ACP-ISD11 complex was fixed to a NUNC MaxiSorp multiwell plate. Wells were blocked using blocking buffer provided by QIAGEN and subsequently incubated with NFS1. Human NFS1 was expressed in *E. coli* and purified in the absence of ISD11. An extensive washing (buffer 20 mM Tris-HCl, 150 mM NaCl, pH 7.5) was carried out to prevent the unspecific binding of the enzyme. Finally, detection of NFS1 was carried out by incubation (1 h) with anti RGSHHHH mAB, which recognizes the epitope RGSHHHH uniquely present in NFS1 (neither the G nor the first H residue are replaceable at all by other amino acids); the mAB was conjugated to the peroxidase enzyme. Bound NFS1 was revealed by means of measurements of peroxidase activity using 3,3′,5,5′-tetramethylbenzidine (TMB) as the substrate. The reaction was stopped by the addition of 0.4 N sulfuric acid. The reaction product was measured by the increment in absorbance at 450 nm using a Sunrise plate reader from TECAN.

Determination of Cysteine Desulfurase Activity. The enzymatic desulfurization of cysteine to alanine and sulfide by the NFS1/ACP-ISD11 complex was determined by the methylene blue method. Concentrations of proteins, substrate, and reducing agent were set according to a previous work by Tsai and Barondeau.[12] Reactions contained 1.0 μM NFS1, 1.0 μM ACP-ISD11, 3.0 μM FXN, and 3.0 μM ISCU. Samples were supplemented with 10 μM PLP, 2 mM DTT, and 1.0 μM Fe^{2+} (final concentrations). The buffer was 50 mM Tris-HCl and 200 mM NaCl, at pH 8.0. A reaction was started by the addition of 1 mM cysteine, and samples were incubated at RT for 30 min. Sulfide production was stopped by the addition of 50 μL of 20 mM N,N-dimethyl p-phenylenediamine in 7.2 N HCl and 50 μL of 30 mM $FeCl_3$ (prepared in 1.2 N HCl). Under these conditions, methylene blue production took 20 min. After that, the samples were centrifuged for 5 min at 12 000*g*, and the supernatant was separated. Absorbance at 670 nm was measured.

Mass Spectrometry and Protein Sequencing. Protein identity was verified by mass analysis, using LCQ DUO ESI ion trap (Thermo Finnigan) or QExactive Orbitrap (Thermo Scientific) spectrometers. N-terminal sequencing of the protein was carried out by automated Edman degradation. Experiments were performed in the National Laboratory of Research and Services in Peptides and Proteins and Mass Spectrometry - LANAIS PROEM - UBA CONICET.

ASSOCIATED CONTENT

Supporting Information

The Supporting Information is available free of charge on the ACS Publications website at DOI: 10.1021/acschembio.8b00184.

Figures S1−S11, information concerning controlled proteolysis of ACP-ISD11 complex with chymotrypsin, information concerning protein sequences (PDF)

AUTHOR INFORMATION

Corresponding Author

*Telephone: +54 114 964 8289 ext. 108. Fax: +54 114 962 5457. E-mail: javiersantosw@gmail.com.

ORCID

María Georgina Herrera: 0000-0002-8874-7410

Javier Santos: 0000-0002-1140-8234

Funding

This study was supported by the Agencia Nacional de Promoción Científica y Tecnológica (ANPCyT PICT2013 Nro.0983), the Consejo Nacional de Investigaciones Científicas y Técnicas (CONICET), the Universidad de Buenos Aires

DOI: 10.1021/acschembio.8b00184
ACS Chem. Biol. XXXX, XXX, XXX−XXX

(UBACyT2014 20020130100468BA), and FARA, Friedreich's Ataxia Research Alliance.

Notes

The authors declare no competing financial interest.

■ ACKNOWLEDGMENTS

M.G.H. thanks Bunge-Born foundation for her fellowship. M.F.P. thanks FARA Alliance for her fellowship. M.E.N. and J.S. thank CONICET for the financial support.

■ REFERENCES

(1) Beilschmidt, L. K., and Puccio, H. M. (2014) Mammalian Fe-S cluster biogenesis and its implication in disease. *Biochimie 100*, 48−60.
(2) Braymer, J. J., and Lill, R. (2017) Iron-sulfur cluster biogenesis and trafficking in mitochondria. *J. Biol. Chem. 292*, 12754−12763.
(3) Lim, S. C., Friemel, M., Marum, J. E., Tucker, E. J., Bruno, D. L., Riley, L. G., Christodoulou, J., Kirk, E. P., Boneh, A., DeGennaro, C. M., Springer, M., Mootha, V. K., Rouault, T. A., Leimkuhler, S., Thorburn, D. R., and Compton, A. G. (2013) Mutations in LYRM4, encoding iron-sulfur cluster biogenesis factor ISD11, cause deficiency of multiple respiratory chain complexes. *Hum. Mol. Genet. 22*, 4460−4473.
(4) Puccio, H., Anheim, M., and Tranchant, C. (2014) Pathophysiological and therapeutic progress in Friedreich ataxia. *Rev. Neurol. 170*, 355−365.
(5) Legati, A., Reyes, A., Ceccatelli Berti, C., Stehling, O., Marchet, S., Lamperti, C., Ferrari, A., Robinson, A. J., Muhlenhoff, U., Lill, R., Zeviani, M., Goffrini, P., and Ghezzi, D. (2017) A novel de novo dominant mutation in ISCU associated with mitochondrial myopathy. *J. Med. Genet. 54*, 815−824.
(6) Nordin, A., Larsson, E., and Holmberg, M. (2012) The defective splicing caused by the ISCU intron mutation in patients with myopathy with lactic acidosis is repressed by PTBP1 but can be derepressed by IGF2BP1. *Hum. Mutat. 33*, 467−470.
(7) Olsson, A., Lind, L., Thornell, L. E., and Holmberg, M. (2008) Myopathy with lactic acidosis is linked to chromosome 12q23.3−24.11 and caused by an intron mutation in the ISCU gene resulting in a splicing defect. *Hum. Mol. Genet. 17*, 1666−1672.
(8) Saha, P. P., Kumar, S. K., Srivastava, S., Sinha, D., Pareek, G., and D'Silva, P. (2014) The presence of multiple cellular defects associated with a novel G50E iron-sulfur cluster scaffold protein (ISCU) mutation leads to development of mitochondrial myopathy. *J. Biol. Chem. 289*, 10359−10377.
(9) Farhan, S. M., Wang, J., Robinson, J. F., Lahiry, P., Siu, V. M., Prasad, C., Kronick, J. B., Ramsay, D. A., Rupar, C. A., and Hegele, R. A. (2014) Exome sequencing identifies NFS1 deficiency in a novel Fe-S cluster disease, infantile mitochondrial complex II/III deficiency. *Mol. Genet. Genomic Med. 2*, 73−80.
(10) Pandolfo, M., and Pastore, A. (2009) The pathogenesis of Friedreich ataxia and the structure and function of frataxin. *J. Neurol. 256* (Suppl 1), 9−17.
(11) Richards, T. A., and van der Giezen, M. (2006) Evolution of the Isd11-IscS complex reveals a single alpha-proteobacterial endosymbiosis for all eukaryotes. *Mol. Biol. Evol. 23*, 1341−1344.
(12) Tsai, C.-L., and Barondeau, D. P. (2010) Human Frataxin Is an Allosteric Switch That Activates the Fe−S Cluster Biosynthetic Complex. *Biochemistry 49*, 9132−9139.
(13) Colin, F., Martelli, A., Clémancey, M., Latour, J.-M., Gambarelli, S., Zeppieri, L., Birck, C., Page, A., Puccio, H., and Ollagnier de Choudens, S. (2013) Mammalian Frataxin Controls Sulfur Production and Iron Entry during de Novo Fe4S4 Cluster Assembly. *J. Am. Chem. Soc. 135*, 733−740.
(14) Parent, A., Elduque, X., Cornu, D., Belot, L., Le Caer, J.-P., Grandas, A., Toledano, M. B., and D'Autréaux, B. (2015) Mammalian frataxin directly enhances sulfur transfer of NFS1 persulfide to both ISCU and free thiols. *Nat. Commun. 6*, 5686.
(15) Webert, H., Freibert, S.-A., Gallo, A., Heidenreich, T., Linne, U., Amlacher, S., Hurt, E., Mühlenhoff, U., Banci, L., and Lill, R. (2014) Functional reconstitution of mitochondrial Fe/S cluster synthesis on Isu1 reveals the involvement of ferredoxin. *Nat. Commun. 5*, 5013.
(16) Cai, K., Tonelli, M., Frederick, R. O., and Markley, J. L. (2017) Human Mitochondrial Ferredoxin 1 (FDX1) and Ferredoxin 2 (FDX2) Both Bind Cysteine Desulfurase and Donate Electrons for Iron-Sulfur Cluster Biosynthesis. *Biochemistry 56*, 487−499.
(17) Tong, W. H., and Rouault, T. A. (2006) Functions of mitochondrial ISCU and cytosolic ISCU in mammalian iron-sulfur cluster biogenesis and iron homeostasis. *Cell Metab. 3*, 199−210.
(18) Liu, G., Wang, Y., Anderson, G. J., Camaschella, C., Chang, Y., and Nie, G. (2016) Functional Analysis of GLRX5Mutants Reveals Distinct Functionalities of GLRX5 Protein. *J. Cell. Biochem. 117*, 207−217.
(19) Banci, L., Brancaccio, D., Ciofi-Baffoni, S., Del Conte, R., Gadepalli, R., Mikolajczyk, M., Neri, S., Piccioli, M., and Winkelmann, J. (2014) [2Fe-2S] cluster transfer in iron−sulfur protein biogenesis. *Proc. Natl. Acad. Sci. U. S. A. 111*, 6203−6208.
(20) Kim, J. H., Alderson, T. R., Frederick, R. O., and Markley, J. L. (2014) Nucleotide-dependent interactions within a specialized Hsp70/Hsp40 complex involved in Fe-S cluster biogenesis. *J. Am. Chem. Soc. 136*, 11586−11589.
(21) Boniecki, M. T., Freibert, S. A., Muhlenhoff, U., Lill, R., and Cygler, M. (2017) Structure and functional dynamics of the mitochondrial Fe/S cluster synthesis complex. *Nat. Commun. 8*, 1287.
(22) Cory, S. A., Van Vranken, J. G., Brignole, E. J., Patra, S., Winge, D. R., Drennan, C. L., Rutter, J., and Barondeau, D. P. (2017) Structure of human Fe-S assembly subcomplex reveals unexpected cysteine desulfurase architecture and acyl-ACP-ISD11 interactions. *Proc. Natl. Acad. Sci. U. S. A. 114*, E5325−E5334.
(23) Friemel, M., Marelja, Z., Li, K., and Leimkühler, S. (2017) The N-Terminus of Iron−Sulfur Cluster Assembly Factor ISD11 Is Crucial for Subcellular Targeting and Interaction with l-Cysteine Desulfurase NFS1. *Biochemistry 56*, 1797−1808.
(24) Cai, K., Frederick, R. O., Tonelli, M., and Markley, J. L. (2017) Mitochondrial Cysteine Desulfurase and ISD11 Coexpressed in Escherichia coli Yield Complex Containing Acyl Carrier Protein. *ACS Chem. Biol. 12*, 918−921.
(25) Saha, P. P., Srivastava, S., Kumar, S. K. P., Sinha, D., and D'Silva, P. (2015) Mapping Key Residues of ISD11 Critical for NFS1-ISD11 Subcomplex Stability: Implications in the development of mitochondrial disorder, COXP19. *J. Biol. Chem. 290*, 25876−25890.
(26) Wiedemann, N., Urzica, E., Guiard, B., Muller, H., Lohaus, C., Meyer, H. E., Ryan, M. T., Meisinger, C., Muhlenhoff, U., Lill, R., and Pfanner, N. (2006) Essential role of Isd11 in mitochondrial iron-sulfur cluster synthesis on Isu scaffold proteins. *EMBO J. 25*, 184−195.
(27) Angerer, H., Schonborn, S., Gorka, J., Bahr, U., Karas, M., Wittig, I., Heidler, J., Hoffmann, J., Morgner, N., and Zickermann, V. (2017) Acyl modification and binding of mitochondrial ACP to multiprotein complexes. *Biochim. Biophys. Acta, Mol. Cell Res. 1864*, 1913−1920.
(28) Van Vranken, J. G., Jeong, M. Y., Wei, P., Chen, Y. C., Gygi, S. P., Winge, D. R., and Rutter, J. (2016) The mitochondrial acyl carrier protein (ACP) coordinates mitochondrial fatty acid synthesis with iron sulfur cluster biogenesis, *eLife 5*, DOI: 10.7554/eLife.17828.
(29) Marsh, J. A., and Forman-Kay, J. D. (2010) Sequence determinants of compaction in intrinsically disordered proteins. *Biophys. J. 98*, 2383−2390.
(30) Micsonai, A., Wien, F., Kernya, L., Lee, Y. H., Goto, Y., Refregiers, M., and Kardos, J. (2015) Accurate secondary structure prediction and fold recognition for circular dichroism spectroscopy. *Proc. Natl. Acad. Sci. U. S. A. 112*, E3095−3103.
(31) Frishman, D., and Argos, P. (1995) Knowledge-based protein secondary structure assignment. *Proteins: Struct., Funct., Genet. 23*, 566−579.
(32) Huynh, K., and Partch, C. L. (2015) Analysis of protein stability and ligand interactions by thermal shift assay. *Curr. Protoc Protein Sci. 79*, 28.9.1.

DOI: 10.1021/acschembio.8b00184
ACS Chem. Biol. XXXX, XXX, XXX−XXX

(33) Yan, R., Friemel, M., Aloisi, C., Huynen, M., Taylor, I. A., Leimkuhler, S., and Pastore, A. (2016) The Eukaryotic-Specific ISD11 Is a Complex-Orphan Protein with Ability to Bind the Prokaryotic IscS. *PLoS One 11*, e0157895.
(34) Fox, N. G., Das, D., Chakrabarti, M., Lindahl, P. A., and Barondeau, D. P. (2015) Frataxin Accelerates [2Fe-2S] Cluster Formation on the Human Fe-S Assembly Complex. *Biochemistry 54*, 3880−3889.
(35) Parent, A., Elduque, X., Cornu, D., Belot, L., Le Caer, J. P., Grandas, A., Toledano, M. B., and D'Autreaux, B. (2015) Mammalian frataxin directly enhances sulfur transfer of NFS1 persulfide to both ISCU and free thiols. *Nat. Commun. 6*, 5686.
(36) Bridwell-Rabb, J., Iannuzzi, C., Pastore, A., and Barondeau, D. P. (2012) Effector role reversal during evolution: the case of frataxin in Fe-S cluster biosynthesis. *Biochemistry 51*, 2506−2514.
(37) Angerer, H. (2015) Eukaryotic LYR Proteins Interact with Mitochondrial Protein Complexes. *Biology (Basel, Switz.) 4*, 133−150.
(38) Angerer, H. (2013) The superfamily of mitochondrial Complex1_LYR motif-containing (LYRM) proteins. *Biochem. Soc. Trans. 41*, 1335−1341.
(39) Brown, A., Rathore, S., Kimanius, D., Aibara, S., Bai, X. C., Rorbach, J., Amunts, A., and Ramakrishnan, V. (2017) Structures of the human mitochondrial ribosome in native states of assembly. *Nat. Struct. Mol. Biol. 24*, 866−869.
(40) Dobrynin, K., Abdrakhmanova, A., Richers, S., Hunte, C., Kerscher, S., and Brandt, U. (2010) Characterization of two different acyl carrier proteins in complex I from Yarrowia lipolytica. *Biochim. Biophys. Acta, Bioenerg. 1797*, 152−159.
(41) Angerer, H., Radermacher, M., Mankowska, M., Steger, M., Zwicker, K., Heide, H., Wittig, I., Brandt, U., and Zickermann, V. (2014) The LYR protein subunit NB4M/NDUFA6 of mitochondrial complex I anchors an acyl carrier protein and is essential for catalytic activity. *Proc. Natl. Acad. Sci. U. S. A. 111*, 5207−5212.

DOI: 10.1021/acschembio.8b00184
ACS Chem. Biol. XXXX, XXX, XXX−XXX